ACS APPLIED MATERIALS & INTERFACES

Research Article

www.acsami.org

Silica Nanoparticles and Frameworks from Rice Husk Biomass

Weixing Wang,*[,†] Jarett C. Martin,[‡] Xiaotian Fan,[†] Aijie Han,[§] Zhiping Luo,[⊥] and Luyi Sun*[,‡]

[†]School of Chemistry and Chemical Engineering, South China University of Technology, Guangzhou, China 510640

[‡]Department of Chemistry and Biochemistry & Materials Science and Engineering Program, Texas State University−San Marcos, San Macros, Texas 78666, United States

[§]Department of Chemistry, The University of Texas-Pan American, Edinburg, Texas 78539-2999, United States

[⊥]Microscopy and Imaging Center & Materials Science and Engineering Program, Texas A&M University, College Station, Texas 77843, United States

ABSTRACT: Biogenic silica nanoparticles (25−30 nm in diameter) were synthesized from rice husks. The characterizations revealed that the silica nanoparticles were composed of smaller primary particles (ca. 4.2 nm in diameter), and their clustering led to a porous structure with a surface area of 164 m^2/g. Under the controlled melting catalyzed by K^+, such silica nanoparticle clusters can gradually fuse to form semicrystalline porous silica frameworks with tunable pore size and structural integrity.

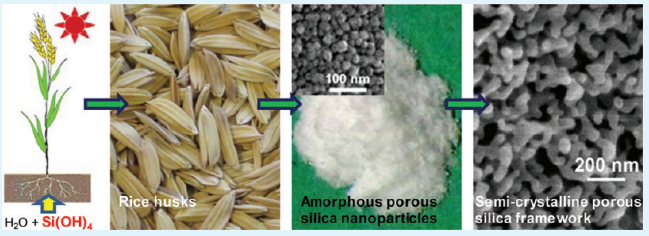

KEYWORDS: *silica nanoparticles, rice husk, porous, biomass, hierarchical*

INTRODUCTION

Silica is a very important industrial material and has found widespread applications.[1,2] In particular, silica nanoparticles with high surface area (porous and/or with a small particle size), are of high interest to many key chemical applications, such as sorption, insulating, sensing, separation, and catalysis.[3,4] Recently, porous silica for biomedical applications, such as controlled release and biosensing, have also been explored.[5,6]

Many approaches have been developed to synthesize porous silica and silica nanoparticles. Usually, a silica precursor, such as silicon alkoxide (typically silicon tetraethoxysilane) is used as the silicon source.[7−10] While such methods are effective to synthesize various silicas with controlled particle size, morphology, and porosity, their main disadvantages are the cost and sustainability issues associated with the silica precursors. Silicon alkoxides are typically synthesized from a multistep reaction route starting from the carbothermal reduction of raw silica, such as sand.[10−12] Such chemical processes are energy intensive and associated with high temperature, high pressure, and strong acidity, and are thus eco-hazardous.[13] Considering the ever increasing demand on porous silica and silica nanoparticles for new applications,[7,9] the current approach to synthesize porous silica and silica nanoparticles may not be sustainable and not match the cost requirement. Thus, it is highly desirable to seek an alternative approach that is more economical and environmentally benign.

The occurrence of silica in a wide range of biological system has been well-known and investigated.[14,15] In particular, the biomineralization of silica in diatoms,[16−18] the unicellular photosynthetic organisms, which leads to the formation of numerous hierarchical nanostructured silica, has inspired extensive studies to prepare similar nanostructured silica in lab.[19−21] Although more than 10 000 species of diatoms with unique shape and structure of their silica based shells have been known, to mimic the silica biomineralization via in vitro materials bioengineering is still a challenge.[18] Another typical example of biomineralization of silica is the formation of silica cell wall in rice husks (RHs).[22−25] Although the silica structures from RHs appear to be much less complicated and less visually attractive compared to the ones from diatoms, the large quantities of RH biomass offer an opportunity for mass production of nanostructured silica for industrial applications. RHs typically contain 20−22% total weight of rice grains.[13] In 2007, the estimated global rice production is ca. 650 million tons.[26] However, owing to their tough, abrasive nature, low nutritive properties, great bulk, and high ash content, efforts to utilize RHs have been very limited. In some countries, RHs have to be disposed with additional cost, and even leading to pollution issues.[27] Harvesting silica from RHs can not only take full advantage of the highest possible value from RH biomass, but also minimize the related environmental issues from the current applications/disposals of RHs.

In RHs, silica is in hydrated amorphous form[28] and counts up to ca. 20 wt % of dry RH, depending on the variety, climate, and geographic location.[27,29−31] Various approaches to extract silica from RHs have been explored.[27] Although the earlier work mainly focused on the purity of the obtained silica, the morphology and microstructure of RH silica have been largely ignored.[27] In this research, we intend to explore the intrinsic morphology and microstructure of the biogenic silica in RH by

Received: November 19, 2011
Accepted: December 29, 2011
Published: December 29, 2011

controlling the pretreatment and reaction conditions to maintain their original structure. Silica nanoparticles with narrow size distribution and high surface area were synthesized. Moreover, such silica nanoparticles could be subsequently converted to semicrystalline porous silica frameworks with tunable pore size, which may find wide applications because of the increased crystallinity and structural integrity. Overall, we present an economical alternative approach to synthesize high-quality silica nanoparticles and porous frameworks from RH biomass.

EXPERIMENTAL SECTION

The RHs used in this research were obtained from Guangdong Academy of Agricultural Science. Analytical reagent grade hydrochloride acid (37 wt %) and KNO_3 were ordered from Alfa Aesar, both of which were used as received.

The raw RHs were boiled in 10 wt % HCl solution for 2 h, rinsed with deionized water, and then dried at 100 °C for 24 h. The dried RHs were then pyrolyzed in a muffle furnace, which was preheated to 700 °C, for 2 h to prepare silica nanoparticles. A control sample was prepared via the same pyrolysis condition but using water rinsed RHs instead of HCl treatment. The silica nanoparticles synthesized from the pyrolysis were then ultrasonicated in 0.20 and 0.50 M KNO_3 solution, respectively, followed by 1 h of stirring. The samples were then filtered and dried at 105 °C for 4 h. The dried samples were subsequently pyrolyzed at 800 °C for 2, 4, and 8 h to form semicrystalline porous silica framework.

Scanning electron microscopy (SEM) images were acquired on a JEOL JSM 6330F field emission-SEM (FE-SEM). The samples were sputter coated with a thin layer (ca. 3 nm) of Au/Pd prior to SEM imaging. Transmission electron microscopy (TEM) imaging was carried out using a FEI Tecnai G^2 F20 with field emission gun (FEG), at a working voltage of 200 kV. Observations were made through the holes of the carbon support film, so that no noise from the support film was introduced.

Small angle X-ray scattering (SAXS) experiments were performed on a Rigaku D/MAX-1200/2203F5 small angle apparatus with a scattering angle 2θ of 0.1−3.0°. Scattered X-ray intensity $I(q)$ was recorded as a function of the scattering wave vector q ($q = 4\pi\sin\theta/\lambda$, λ = 0.1540 nm, the wavelength of the incident X-ray). The surface area and porosity of the selected silica samples were characterized using a Micromeritics' Accelerated Surface Area and Porosimetry (ASAP) 2020 analyzer (Atlanta, Georgia, USA) by N_2 sorption at 77 K. The samples were dried at 100 °C for 12 h prior to the test. X-ray diffraction (XRD) patterns were recorded using a Bruker D8 diffractometer with Bragg−Brentano θ-2θ geometry (20.0 kV and 5.0 mA), using a graphite monochromator with Cu Kα radiation.

RESULTS AND DISCUSSION

In addition to hydrated silica,[27,28] RHs are mainly composed of cellulose, hemicellulose, and lignin,[32,33] and low concentrations of various metal cations.[27] Although the organic components can be removed by thermal decomposition, care must be exercised since some metal cations, especially K^+, were reported to be able to catalyze the melting of silica.[34−39] Therefore, RHs were first boiled in 10 wt % HCl solution for 2 h to remove most of the metal cations. Silica nanoparticles were successfully obtained by pyrolyzing the HCl treated RHs at 700 °C for 2 h. As shown in Figure 1A, the synthesized silica nanoparticles possess narrow size distribution of ca. 25−30 nm. The XRD pattern (as shown in Figure 5, which will be further discussed below) clearly shows that such silica nanoparticles are amorphous. In contrast, the sample synthesized via the same reaction condition but using water rinsed RHs exhibited significant aggregation (as shown in Figure 1B), because of the K^+ catalyzed melting of silica as discussed above.[34−39]

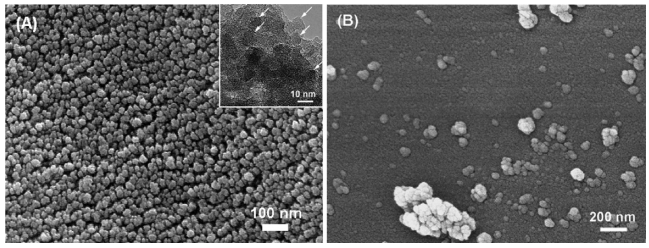

Figure 1. (A) SEM image of silica nanoparticles synthesized from HCl treated RHs. The inset shows the observation of smaller primary particles under TEM, as illustrated by the arrows. (B) SEM image of silica particle agglomerates synthesized from the water rinsed RHs.

Although HCl pretreatment is shown to be effective to remove metal cations to minimize the aggregation of silica nanoparticles, potentially allowing the resultant silica to maintain its original structure in cell wall, the SEM characterization could only disclose the formation of silica nanoparticles. It is hard to further magnify to observe more detailed microstructure within individual nanoparticles because of the resolution limit of SEM. Considering silica typically precipitates on cell walls, in cell lumen, and as extracellular deposits,[25] their biogenic nature indicates that even finer microstructures might exist. To explore potential microstructures within individual nanoparticles, TEM was adopted for further characterization. The TEM inset presented in Figure 1A roughly shows that the 25−30 nm silica nanoparticles are composed of clustering of primary particles with a diameter less than 10 nm. But because the primary particles severely overlap and adhere to each other, it is hard to observe individual primary particles under TEM.

To further investigate the potential microstructures within the silica nanoparticles from RHs, SAXS was selected. SAXS is a primary tool to investigate the structure of mass fractal aggregates since it can probe structure over several orders in length scale, which includes both the primary particles and fractal aggregates.[40] Mass fractal aggregates show three defining features in $I(q)$ versus q scattering data plotted on natural log−natural log scale: a power law ($I(q) \sim q^{D_s-6}$) region corresponding to the surface scattering from the primary particles; a second power law region ($I(q) \sim q^{-D_m}$) at lower q values corresponding to the scattering from the aggregates; and a curved crossover region between the two power laws.[41−43] This crossover region occurs at q value (q_c) of the order of $1/a$, where a is the radius of the primary particles.[41−43] The exponent D_m can be interpreted as a fractal dimension, which is a measure of the branching of the particle aggregates. The exponent (D_s-6) gives information about the surface structure of the primary particles. Smooth particles have a surface-fractal dimension $D_s = 2$, which cause a Porod-decay ($I(q) \sim q^{-4}$); while rough particles give slopes between −3 and −4.[41−43] Unlike TEM, which focuses on selected particles, SAXS offers an advantage to give statistical information from a large amount of sample. As shown in Figure 2, two regimes of power-low scattering can be observed in the measured SAXS pattern presented in the natural log−natural log plot. The results indicate that the primary particle diameter of the silica nanoparticles is about 4.2 nm ($2a \approx 4.2$ nm). Its surface fractal dimension D_s is about 2.1, indicating the presence of a relatively smooth surface for the primary particles. The mass fractal dimension D_m is about 2.8, showing the self-similar property of these silica nanoparticles. The D_m value of 2.8 is reasonable for a 3-dimentional fractal aggregate.

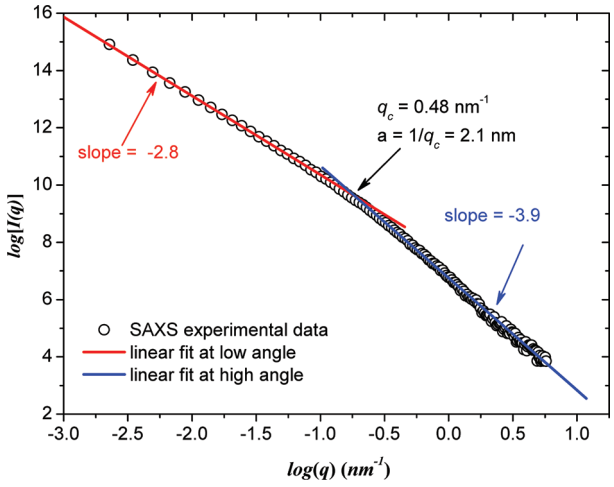

Figure 2. SAXS pattern of silica nanoparticles from RH biomass.

The surface area characterization (Figure 3) further revealed that such silica nanoparticles have a Brunauer–Emmett–Teller

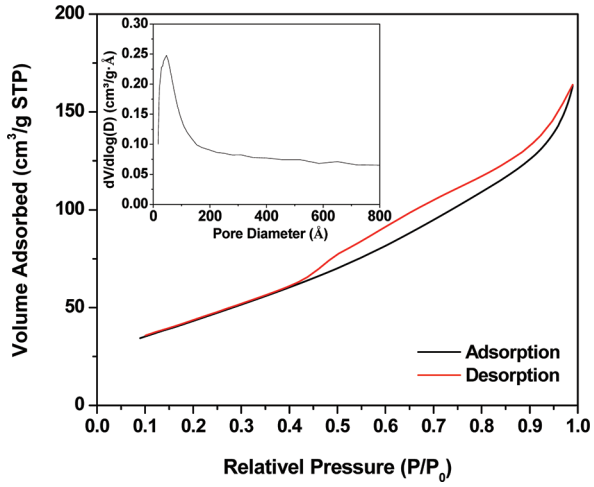

Figure 3. N_2 sorption isotherms of porous silica nanoparticles. The inset shows the pore size distribution obtained from BJH adsorption.

(BET) surface area of 164 m^2/g. If the silica nanoparticles (with a diameter of ca. 25–30 nm) were solid (nonporous), they should have a specific surface area of ca. 90–108 m^2/g (assuming the particles are spherical and without any surface contact among particles, and the density of amorphous silica is 2.22 g/cm^3).[44] Thus, the result of the BET surface area test proved that those 25–30 nm silica nanoparticles were actually porous, which was also consistent with the above TEM and SAXS characterizations. The Barret-Joyner-Halenda (BJH) analysis, as shown in the inset of Figure 3, revealed that such silica nanoparticles possess a group of pores with a diameter mainly ranging from ca. 2.0–9.0 nm, which is believed to be contributed by the gaps between the primary particles. In brief, the surface area and porosity characterization supplements the TEM and SAXS results, suggesting that the 25–30 nm silica nanoparticles are composed of smaller primary particles with a diameter of ca. 4.2 nm. Those primary silica nanoparticles cluster to form a porous structure.

The porous structure of RH silica, as confirmed by the BET/BJH characterization discussed above, is possibly originated from the limited marginal melting of primary silica nanoparticles during the synthesis. As aforementioned, RHs contain potassium cations, which can catalyze the melting of silica during pyrolysis, generating severe aggregation[34−39] as shown in Figure 1B. Although HCl treatment can effectively remove majority of potassium cations, a trace amount of potassium cations might remain even after HCl leaching, which could be the cause for the clustering of primary nanoparticles to form porous silica nanoparticles.

This potential cause inspires us to generate a secondary porous structure by further partially melting the silica nanoparticles. Ideally, one might be able to fabricate ordered porous structure by tailoring the pretreatment of the synthesized nanoparticles and subsequent pyrolysis conditions.

On the basis of the above motivations, two samples of the synthesized silica nanoparticles were treated by KNO_3 solutions and subsequently treated under various conditions following the procedures detailed in the Experimental Section. The purpose for KNO_3 treatment is to introduce K^+ cations into the porous structure of silica nanoparticles, which should promote the melting of silica nanoparticles to form porous structure. It was observed that upon contact with a drop of KNO_3 solution, the porous silica nanoparticles can quickly absorb the solution drop. It is expected that the different concentrations of KNO_3 will lead to different levels of doping of K^+ cations in silica nanoparticles, which will result in different degrees of melting and thus different pore structures and pore sizes. Figure 4

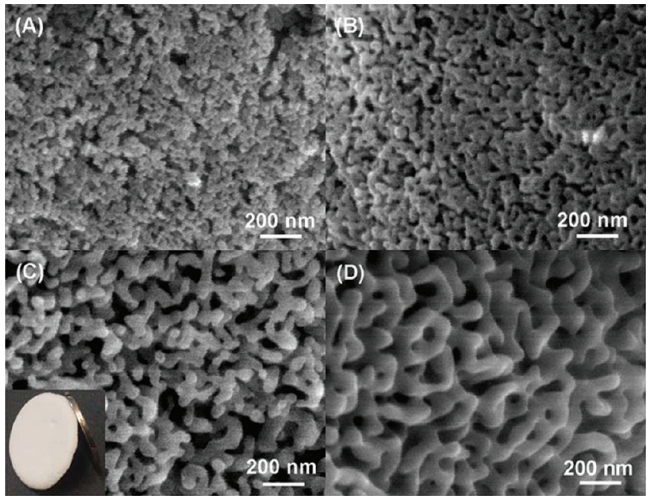

Figure 4. SEM images of meso/macroporous silica frameworks: (A) 0.20 M KNO_3, pyrolysis at 800 °C for 2 h; (B) 0.20 M KNO_3, pyrolysis at 800 °C for 4 h; (C) 0.20 M KNO_3, pyrolysis at 800 °C for 8 h; (D) 0.50 M KNO_3, pyrolysis at 800 °C for 8 h. The inset in C shows a coin shaped disk made of the corresponding semicrystalline porous silica framework.

shows the SEM images of a series of porous silica framework synthesized from the above KNO_3 treated samples pyrolyzed at 800 °C for various durations. Figure 4A–C clearly shows the gradual melting and pore structure formation progress of 0.20 M KNO_3 solution treated silica nanoparticles. After 2 h of pyrolysis at 800 °C, the silica nanoparticles started to stick together. After 4 h of treatment, the nanoparticles began to fuse and form porous structure, with a pore size of ca. 20 nm. After 8 h of synthesis, well-defined pore structure formed, with pore size ranging from ca. 25–40 nm. Treatment with a higher concentration of KNO_3 solution (0.50 M) apparently led to more pronounced fusing of silica nanoparticles. Although the

dx.doi.org/10.1021/am201619u | ACS Appl. Mater. Interfaces 2012, 4, 977–981

pore size did not change much compared to the 0.20 M KNO_3 treated sample, it led to the formation of much thicker wall (Figure 4D). These results confirm the above hypothesis that one may tailor the pretreatment and pyrolysis condition to synthesize meso/macroporous silica from RHs with tunable structures. It should be noted that such secondary porous silica is semicrystalline. As shown in Figure 5, the 25−30 nm silica

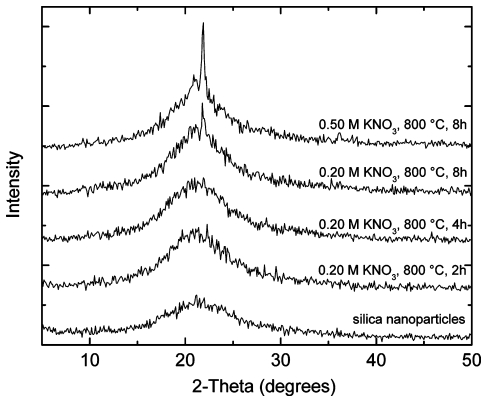

Figure 5. XRD patterns of KNO_3 solution treated silica nanoparticles.

nanoparticles from RHs are initially amorphous. Extended pyrolysis of 0.20 M KNO_3 solution treated silica nanoparticle at 800 °C gradually enhanced the sample crystallinity. While the 0.50 M KNO_3 solution treated silica nanoparticle exhibited even higher degree of crystallinity under the same pyrolysis treatment. More importantly, with increasing crystallinity, the silica nanoparticles can be processed to form any desirable shape, and possess sufficient structural integrity (a coin shaped disk as an example is presented in the inset of Figure 4C). Thus, they might find wider applications and exhibit superior performance compared to amorphous porous silica, such as filtering, etc. While this work focuses on exploring the possibility to form semicrystalline porous silica framework via controlled fuse of silica nanoparticles, more detailed research is underway to fine-tune the pore size and structure using various dopants and reaction conditions, which will be reported later.

To explain the hierarchical structure of the porous silica nanoparticles synthesized from RHs, and their melting progress and porous framework formation, we propose a model as shown in Figure 6.

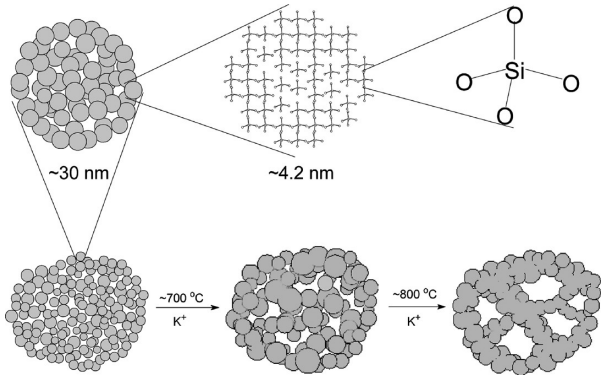

Figure 6. Hierarchical structure model of silica nanoparticles synthesized from RHs and the formation mechanism of porous silica framework.

The above characterization results have suggested that the silica nanoparticles prepared from RH biomass are composed of amorphous silica. The diameter of the primary particles is ca. 4.2 nm according to the SAXS characterization. At the next level, primary particles cluster to form larger secondary particles with a diameter of ca. 25−30 nm, as imaged under SEM (Figure 1A). The mass fractal dimension is about 2.8 showing 3-dimensional self-similar property over the range of ca. 4.2 to 25−30 nm. At the next level, the secondary particles bundle to form large clusters. Under elevated temperatures, particularly at the presence of potassium cations, the silica particles gradually melt and fuse together to form larger aggregates and subsequently to form porous structures (and eventually to form silica bulk with sufficiently long heating). Their amorphous morphology converts to semicrystalline gradually during the process.

This work represents a fine example to replicate the microstructure of mineral in living organism and derive value added products from biomass. While many chemicals have been successfully derived from biomass, in many cases the feedstock is food, such as polylactic acid from corn,[45] and ethanol from sugar cane or grain.[46] But in this case, RH biomass with little value (sometimes even considered as biowaste) was the starting material, which offers an advantage for further development toward commercialization.

CONCLUSIONS

In conclusion, biogenic porous silica nanoparticles with a diameter of ca. 25−30 nm were successfully prepared from HCl-treated RH biomass via controlled pyrolysis. The SAXS and surface area characterizations further showed that the silica nanoparticles were composed of smaller primary particles, and the clustering of the primary particles leads to porous structure. More importantly, by doping the synthesized silica nanoparticles with K^+ cations and tailoring pyrolysis conditions, the silica nanoparticles can be further converted to semicrystalline meso/macroporous frameworks with tunable pore size. Their high surface area, low cost, and appreciable structure integrity may lead to many new applications in the near future.

AUTHOR INFORMATION

Corresponding Author

*Tel:86-20-22236985 (W.W.); (512) 245-5563 (L.S.). Fax: 86-20-22236985 (W.W.); (512) 245-2374 (L.S.). E-mail: cewxwang@scut.edu.cn (W.W.); luyi.sun@txstate.edu (L.S.).

ACKNOWLEDGMENTS

This research is sponsored by the U.S. Environmental Protection Agency's P3 Award (SU-83508401) and the U.S. Department of Agriculture (2011-38422-30803). W.W. thanks the support by the Fundamental Research Funds for the Central Universities (2011ZM0046) and the National Natural Science Foundation of China (1176093). L.S. acknowledges the start-up fund and the Research Enhancement Grant from Texas State University-San Marcos, the Research Corporation for Science Advancement, and the Welch Foundation for partial support for this research. We thank Prof. Kecheng Gong for valuable discussions.

REFERENCES

(1) Glasser, F. P. In *Encyclopedia of Materials Science and Engineering*; Beaver, M. B., Ed.; The MIT Press: Cambridge, MA, 1986; pp 4393−4401.

(2) Uhrlandt, S. In *Kirk-Othmer Encyclopedia of Chemical Technology*; Seidel, A., Ed.; John Wiley & Sons: Hoboken, NJ, 2006; pp 365−379.
(3) Gurav, J. L.; Jung, I.-K.; Park, H.-H.; Kang, E. S.; Nadargi, D. Y. *J. Nanomater.* **2010**, 1−11.
(4) Pajonk, G. M. *Colloid Polym. Sci.* **2003**, *281*, 637−651.
(5) Trewyn, B. G.; Giri, S.; Slowing, I. I.; Lin, V. S. Y. *Chem. Commun.* **2007**, 3236−3245.
(6) Slowing, I. I.; Trewyn, B. G.; Giri, S.; Lin, V. S. Y. *Adv. Funct. Mater.* **2007**, *17*, 1225−1236.
(7) Soleimani Dorcheh, A.; Abbasi, M. H. *J. Mater. Process. Technol.* **2008**, *199*, 10−26.
(8) Halas, N. J. *ACS Nano* **2008**, *2*, 179−183.
(9) Vivero-Escoto, J. L.; Trewyn, B. G.; Lin, V. S. Y. *Annu. Rev. Nano Res.* **2010**, *3*, 191−231.
(10) Baccile, N.; Babonneau, F.; Thomas, B.; Coradin, T. *J. Mater. Chem.* **2009**, *19*, 8537−8559.
(11) Rösch, L., John, P.; Reitmeier, R. In *Ullmann's Encyclopedia of Industrial Chemistry*; Wiley-VCH: Weinheim, Germany, 2000.
(12) Laine, R. M.; Blohowiak, K. Y.; Robinson, T. R.; Hoppe, M. L.; Nardi, P.; Kampf, J.; Uhm, J. *Nature* **1991**, *353*, 642−644.
(13) Bansal, V.; Ahmad, A.; Sastry, M. *J. Am. Chem. Soc.* **2006**, *128*, 14059−14066.
(14) Perry, C. C. In *Progress in Molecular and Subcellular Biology*; Springer: New York, 2009; pp 295−313.
(15) Ehrlich, H.; Demadis, K. D.; Pokrovsky, O. S.; Koutsoukos, P. G. *Chem. Rev.* **2010**, *110*, 4656−4689.
(16) Brunner, E.; Gröger, C.; Lutz, K.; Richthammer, P.; Spinde, K.; Sumper, M. *Appl. Microbiol. Biotechnol.* **2009**, *84*, 607−616.
(17) Gordon, R.; Losic, D.; Tiffany, M. A.; Nagy, S. S.; Sterrenburg, F. A. S. *Trends Biotechnol.* **2009**, *27*, 116−127.
(18) Sumper, M.; Brunner, E., Wiley-VCH: Weinheim, Germany, 2006; pp 17−26.
(19) Sun, Q.; Vrieling, E. G.; van Santen, R. A.; Sommerdijk, N. A. J. M. *Curr. Opin. Solid State Mater. Sci.* **2004**, *8*, 111−120.
(20) Vrieling, E. G.; Beelen, T. P. M; van Santen, R. A.; Gieskes, W. W. C. *J. Biotechnol.* **1999**, *70*, 39−51.
(21) Kroger, N.; Poulsen, N. *Annu. Rev. Genet.* **2008**, *42*, 83−107.
(22) Mann, S. *Nature* **1993**, *365*, 499−505.
(23) Oliver, S.; Kuperman, A.; Coombs, N.; Lough, A.; Ozin, G. A. *Nature* **1995**, *378*, 47−50.
(24) Mann, S.; Ozin, G. A. *Nature* **1996**, *382*, 313−318.
(25) Ding, T. P.; Ma, G. R.; Shui, M. X.; Wan, D. F.; Li, R. H. *Chem. Geol.* **2005**, *218*, 41−50.
(26) Food and Agriculture Organization (FAO) of the United Nations, 2008.
(27) Sun, L.; Gong, K. *Ind. Eng. Chem. Res.* **2001**, *40*, 5861−5877.
(28) Asuncion, M. J.; Hasegawa, I.; Kampf, J. W.; Laine, R. M. *J. Mater. Chem.* **2005**, *15*, 2114.
(29) Umeda, J.; Kondoh, K.; Michiura, Y. *Mater. Trans.* **2007**, *48*, 3095−3100.
(30) Zhang, H. X.; Zhao, X.; Ding, X. F.; Lei, H.; Chen, X.; An, D. M.; Li, Y. L.; Wang, Z. C. *Bioresour. Technol.* **2010**, *101*, 1263−1267.
(31) Liou, T.-H.; Wu, S.-J. *Ind. Eng. Chem. Res.* **2010**, *49*, 8379−8387.
(32) Markovska, I.; Lyubchev, L. *J. Therm. Anal. Calorim.* **2007**, *89*, 809−814.
(33) Teng, H.; Wei, Y.-C. *Ind. Eng. Chem. Res.* **1998**, *37*, 3806−3811.
(34) Bassett, D. R.; Boucher, E. A.; Zettlemoyer, A. C. *J. Mater. Sci.* **1972**, *7*, 1379−1382.
(35) Kamijo, N.; Umesaki, N. *Jpn. J. Appl. Phys.* **1993**, *32*, 658−660.
(36) Huffman, G. P.; Shah, N.; Zhao, J. M.; Huggins, F. E.; Hoost, T. E.; Halvorsen, S.; Goodwin, J. G. *J. Catal.* **1995**, *151*, 17−25.
(37) Real, C.; Alcalá, M. D.; Muñoz-Páez, A.; Criado, J. M. *Nucl. Instrum. Meth. Phys. Res., Sect. B* **1997**, *133*, 68−72.
(38) Real, C.; Alcalá, M. D.; Criado, J. M. *J. Am. Ceram. Soc.* **1996**, *79*, 2012−2016.
(39) Wang, W.; Martin, J. C.; Zhang, N.; Ma, C.; Han, A.; Sun, L. *J. Nanopart. Res.*,**2011**, *13*, 6981−6990.
(40) Glatter, O.; Kratky, O., Eds.; *Small Angle X-ray Scattering*; Academic Express: London, 1982.
(41) Schaefer, D. W. *Science* **1989**, *243*, 1023−1027.
(42) Schaefer, D. W.; Martin, J. E.; Wiltzius, P.; Cannell, D. S. *Phys. Rev. Lett.* **1984**, *52*, 2371.
(43) Schaefer, D. W.; Keefer, K. D. *Phys. Rev. Lett.* **1984**, *53*, 1383.
(44) National Center for Environmental Assessment, Office of Research and Development, United States Environmental Protection Agency, Research Triangle Park, NC 27711, 1996.
(45) Pang, X. A.; Zhuang, X. L.; Tang, Z. H.; Chen, X. S. *Biotechnol. J* **2010**, *5*, 1125−1136.
(46) Mussatto, S. I.; Dragone, G.; Guimaraes, P. M. R.; Silva, J. P. A; Carneiro, L. M.; Roberto, I. C.; Vicente, A.; Domingues, L.; Teixeira, J. A. *Biotechnol. Adv.* **2010**, *28*, 817−830.